

# Further results on dissimilarity spaces for hyperspectral images RF-CBIR

---

---

# Further results on dissimilarity spaces for hyperspectral images RF-CBIR

Miguel A. Veganzones<sup>a,b,\*</sup>, Mihai Datcu<sup>c,\*\*</sup>, Manuel Graña<sup>a</sup>,

<sup>a</sup>*Grupo de Inteligencia Computacional, Basque Country University (UPV/EHU), Spain*

<sup>b</sup>*Gipsa-lab, Grenoble-INP, France*

<sup>c</sup>*German Aerospace Center (DLR), Germany*

---

## Abstract

Content-Based Image Retrieval (CBIR) systems are powerful search tools in image databases that have been little applied to hyperspectral images. Relevance Feedback (RF) is an iterative process that uses machine learning techniques and user's feedback to improve the CBIR systems performance. We pursued to expand previous research in hyperspectral CBIR systems built on dissimilarity functions defined either on spectral and spatial features extracted by spectral unmixing techniques, or on dictionaries extracted by dictionary-based compressors. These dissimilarity functions were not suitable for direct application in common machine learning techniques. We propose to use a RF general approach based on dissimilarity spaces which is more appropriate for the application of machine learning algorithms to the Hyperspectral RF-CBIR. We validate the proposed RF method for hyperspectral CBIR systems over a real hyperspectral dataset.

*Keywords:* Hyperspectral imaging, CBIR systems, dissimilarity spaces,

---

\*E-mail: miguel-angel.veganzones@gipsa-lab.fr - Phone: +33 (0)476 82 6396

\*\*E-mail: mihai.datcu@dlr.de - Phone: +49 8153 28 1388

E-mail: manuel.grana@ehu.es - Phone: +34 943 01 8044

relevance feedback.

---

## 1 **1. Introduction**

2     The increasing interest in hyperspectral remote sensing [23] will yield  
3 to an exponential growth of hyperspectral data acquisition in a short time.  
4 Most spatial agencies have scheduled the launch of hyperspectral sensors on  
5 satellite payloads such as in EnMAP [6] or PRISMA [9] missions. That will  
6 involve the storage of a huge quantity of hyperspectral data. The problem  
7 of searching through these huge databases using Content-Based Image Re-  
8 trieval (CBIR) techniques has not been properly addressed for the case of  
9 hyperspectral images until recently. Recent works on hyperspectral CBIR  
10 systems [8, 28] make use of spectral and spectral-spatial dissimilarity func-  
11 tions to compare hyperspectral images. The spectral and spatial features are  
12 extracted by means of spectral unmixing algorithms [10]. In [27], authors de-  
13 fine dissimilarity functions built upon Kolmogorov complexity [15] and its ap-  
14 proximation by compression and dictionary distances [29, 14]. Compression-  
15 based distances require a high computational cost that make it unaffordable  
16 for the definition of CBIR systems. Dictionary distances operate over dictio-  
17 naries extracted from the hyperspectral images by the off-line application of  
18 a lossless dictionary-based compressor such as the Lempel-Ziv-Welch (LZW)  
19 compression algorithm [30]. In this work we pursued to extend these hyper-  
20 spectral CBIR systems by using the feedback of the user.

21     Relevance Feedback (RF) is an iterative process that makes use of the  
22 feedback provided by the user to reduce the gap between the low-level fea-  
23 ture representation of the images and the high-level semantics of the user's

24 queries [25]. Often, the user’s feedback comes on the form of a labelling of  
25 the previously retrieved images as relevant or irrelevant for the query. The  
26 set of labelled images is then used by the CBIR system to adapt the search  
27 to the query semantics. If each image is represented by a point in a feature  
28 space, the RF with both, positive and negative training examples, becomes  
29 a two-class classification problem or an online learning problem in a batch  
30 mode [31].

31 Dictionaries and spectral-spatial features extracted from hyperspectral  
32 images cannot be directly represented as points in a feature space. Thus, they  
33 do not fit easily in feature-based machine learning techniques employed for  
34 the definition of RF processes. It is possible to treat dissimilarity functions as  
35 kernel functions in order to use them in kernel-based method, for instance in  
36 Support Vector Machine (SVM) [24]. However, these dissimilarity functions  
37 do not comply often with valid kernel conditions [21]. Authors in [20, 5]  
38 propose the definition of dissimilarity spaces as an alternative to feature  
39 spaces for machine learning. In dissimilarity spaces some data instances are  
40 used as reference points named prototypes. The data samples are compared  
41 to these prototype instances by some dissimilarity function. Then, for each  
42 data sample, the dissimilarities to the prototypes define the data coordinates  
43 in a so-called dissimilarity space. Thus, each prototype defines a dimension  
44 in this dissimilarity space. The dissimilarity space is analogous to a feature  
45 space so, once the data samples are represented as points in the dissimilarity  
46 space, all the available potential of machine learning techniques can then be  
47 used.

48 In this paper we propose the use of dissimilarity spaces to define a RF

49 methodology for hyperspectral CBIR making use of the already available  
50 spectral, spectral-spatial and dictionary dissimilarity functions. The use of  
51 dissimilarity spaces to define RF processes is scarce on the literature. In  
52 [19], authors propose the use of dissimilarities to prototypes selected by an  
53 offline clustering process as the entry to a RF process defined as an one-class  
54 classification problem. Authors in [7] perform an online prototypes selec-  
55 tion instead, where the images retrieved to the user for evaluation are at the  
56 same time the prototypes and the training set. The RF process is defined  
57 as a new dissimilarity function based on the combination of the database  
58 images dissimilarities to the set of prototypes and the prototypes labeling.  
59 In [2], authors propose different strategies to characterize an image by a fea-  
60 ture vector based on the combination of dissimilarities to a set of prototypes.  
61 We propose an hyperspectral RF process defined as a two-class classifica-  
62 tion problem based on dissimilarity spaces. The input to the classifier is a  
63 dissimilarity representation defined over the unmixing and dictionary-based  
64 hyperspectral dissimilarity functions respect to offline and online selected  
65 prototypes.

66 The paper is divided as follows. In section 2 we outline the dissimilarity  
67 functions used in the definition of hyperspectral CBIR systems and in section  
68 3 we outline the dissimilarity spaces approach. In section 4 we introduce the  
69 proposed hyperspectral RF process. In section 5 we define the experimen-  
70 tal methodology and in section 6 we comment on the results. Finally, we  
71 contribute with some conclusions in section 7.

## 72 2. Hyperspectral dissimilarity functions

73 Here, we outline the dissimilarity functions used on the literature to com-  
74 pare hyperspectral images. Firstly, we describe the spectral and spectral-  
75 spatial dissimilarity functions defined over the results of a spectral unmixing  
76 process. Secondly, we describe the dictionary distance defined over dictionar-  
77 ies extracted from the hyperspectral images by means of lossless dictionary-  
78 based compressors.

### 79 2.1. Unmixing-based dissimilarity functions

80 Spectral unmixing pursues the decomposition of an hyperspectral image  
81 into the spectral signatures of its main constituents and their corresponding  
82 spatial fractional abundances. Most of the unmixing methods are based on  
83 the Linear Mixing Model (LMM) [11, 1]. The LMM states that an hyper-  
84 spectral sample is formed by a linear combination of the spectral signatures  
85 of pure materials present in the sample (endmembers), plus some additive  
86 noise. Often, the spectral signatures of the materials are unknown, and the  
87 set of endmembers must be built by either manually selecting spectral sig-  
88 natures from a spectral library, or by automatically inducing them from the  
89 image itself. The latter involves the use of some endmember induction algo-  
90 rithm (EIA). The hyperspectral literature features plenty of such algorithms.  
91 Some reviews on the topic can be found in [22, 26, 1]. Once the set of end-  
92 members has been induced, their corresponding per-pixel abundances can be  
93 estimated by a Least Squares method [12].

94 The dissimilarity functions based on the spectral unmixing make use of  
95 the spectral and spectral-spatial characterization of the hyperspectral im-

96 ages [8, 28]. Given an hyperspectral image,  $\mathbf{H}_\alpha$ , whose pixels are vectors in a  
 97  $q$ -dimensional space, its spectral characterization is defined by the set of end-  
 98 members,  $\mathbf{E}_\alpha = \{\mathbf{e}_1^\alpha, \mathbf{e}_2^\alpha \dots \mathbf{e}_{m_\alpha}^\alpha\}$ , where  $m_\alpha$  denotes the number of induced  
 99 endmembers from the  $\alpha$ -th image. The spectral-spatial characterization is  
 100 defined as the tuple  $(\mathbf{E}_\alpha, \mathbf{\Phi}_\alpha)$ , where  $\mathbf{\Phi}_\alpha = \{\phi_1^\alpha, \phi_2^\alpha, \dots, \phi_{m_\alpha}^\alpha\}$  is the set of  
 101 fractional abundance maps resulting from the unmixing process. To imple-  
 102 ment this approach, an EIA is first used to induce the endmembers from the  
 103 image and then, their respective fractional abundances are estimated by a  
 104 Least Squares Unmixing algorithm.

105 In order to compute the unmixing-based dissimilarities, the Spectral Dis-  
 106 tance Matrix (SDM),  $D_{\alpha,\beta}$ , between two given hyperspectral images,  $H_\alpha$   
 107 and  $H_\beta$ , has first to be computed. The SDM is the matrix  $D_{\alpha,\beta} = [d_{ij}]$ ,  
 108  $i = 1, \dots, m_\alpha, j = 1, \dots, m_\beta$ , whose elements  $d_{ij}$  are the pairwise distances  
 109 between the endmembers  $\mathbf{e}_i^\alpha, \mathbf{e}_j^\beta \in \mathbb{R}^q$  of each image. The spectral distance  
 110 function  $d : \mathbb{R}^q \times \mathbb{R}^q \rightarrow \mathbb{R}^+$  is often the angular pseudo-distance:

$$d(\mathbf{e}_i, \mathbf{e}_j) = \cos^{-1} \frac{\mathbf{e}_i \mathbf{e}_j}{\|\mathbf{e}_i\| \|\mathbf{e}_j\|}. \quad (1)$$

111 The Spectral dissimilarity [8] is then given by:

$$s_{\mathbf{E}}(\mathbf{H}_\alpha, \mathbf{H}_\beta) = \|\mathbf{m}_r\| + \|\mathbf{m}_c\|, \quad (2)$$

112 where  $\|\mathbf{m}_r\|$  and  $\|\mathbf{m}_c\|$  are the Euclidean norms of the vectors of row and  
 113 column minimal values of the SMD, respectively. The Spectral-Spatial dis-  
 114 similarity [28] is given by:

$$s_{\mathbf{E}, \mathbf{\Phi}}(\mathbf{H}_\alpha, \mathbf{H}_\beta) = \sum_{i=1}^{m_\alpha} \sum_{j=1}^{m_\beta} r_{ij} d_{ij}, \quad (3)$$

115 where  $d_{ij}$  is the aforementioned spectral distance and  $r_{ij}$  is the significance  
 116 associated to  $d_{ij}$ . The significance matrix  $R_{\alpha,\beta} = [r_{ij}]$ ,  $i = 1, \dots, m_\alpha$ ,  $j =$   
 117  $1, \dots, m_\beta$  is calculated on base to the normalized average abundances  $\bar{\Phi}_\alpha$   
 118 and  $\bar{\Phi}_\beta$  by the most similar highest priority (MSHP) principle [13].

## 119 2.2. Dictionary-based dissimilarity functions

120 Given a signal  $x$ , a dictionary-based compression algorithm looks for pat-  
 121 terns in the input sequence from signal  $x$ . These patterns, called *words*, are  
 122 subsequences of the incoming sequence. The compression algorithm result  
 123 is a set of unique words called *dictionary*. The dictionary extracted from a  
 124 signal  $x$  is hereafter denoted as  $D(x)$ , with  $D(\lambda) = \emptyset$  only if  $\lambda$  is the empty  
 125 signal. The Normalized Dictionary Distance (NDD) [16] is given by:

$$s_{\text{NDD}}(x, y) = \frac{D(x \cup y) - \min\{D(x), D(y)\}}{\max\{D(x), D(y)\}}, \quad (4)$$

126 where  $D(x \cup y)$  and  $D(x \cap y)$  respectively denote the union and intersection  
 127 of the dictionaries extracted from signals  $x$  and  $y$ . The NDD is a normalized  
 128 admissible distance satisfying the metric inequalities. Thus, it results in a  
 129 non-negative number in the interval  $[0, 1]$ , being zero when the compared  
 130 signals are equal and increasing up to one as the signals are more dissimilar.

## 131 3. Dissimilarity spaces

132 The dissimilarity space is a vector space in which the dimensions are  
 133 defined by dissimilarity vectors measuring pairwise dissimilarities between  
 134 individual objects and reference objects (prototypes) [5]. Given a set of pro-  
 135 totypes  $\mathbf{P} = \{p_1, \dots, p_r\}$ , where  $r$  denotes the number of prototype objects

136 on  $\mathbf{P}$ , and a set of objects  $\mathbf{X} = \{x_1, \dots, x_N\}$ , where  $N$  denotes the num-  
 137 ber of individual objects on  $\mathbf{X}$ , the dissimilarity representation  $D(\mathbf{X}, \mathbf{P})$  is  
 138 a data-dependent mapping  $D(\cdot, \mathbf{P}) : \mathbf{X} \rightarrow \mathfrak{R}^r$  from a set of objects  $\mathbf{X}$  to  
 139 the dissimilarity space specified by the prototypes set  $\mathbf{P}$ . Each dimension  
 140 in the dissimilarity space corresponds to a dissimilarity to a prototype ob-  
 141 ject,  $D(\mathbf{X}, p_i)$ . The dissimilarity representation  $D(\mathbf{X}, \mathbf{P})$  is thus defined as  
 142 a  $N \times r$  dissimilarity matrix, where each object  $\mathbf{x} \in \mathbf{X}$  is described by a  
 143 vector of dissimilarities  $\mathbf{s}_x = D(x, \mathbf{P}) = [s(x, p_1), \dots, s(x, p_r)]$ . The pair-  
 144 wise dissimilarity function  $s(x, p_i)$  is not required to be metric and can be  
 145 defined *ad-hoc* for the given prototype. The dissimilarity space is a vector  
 146 space equipped with an inner product and an Euclidean metric. Thus, the  
 147 vector of dissimilarities to the set of prototypes,  $\mathbf{s}_x$ , can be interpreted as a  
 148 feature, allowing the use of machine learning techniques commonly defined  
 149 over feature spaces.

#### 150 4. Relevance feedback by dissimilarity spaces

151 The use of dissimilarity spaces allows one to use the previously mentioned  
 152 hyperspectral dissimilarity functions to define a RF process based on conven-  
 153 tional machine learning techniques. The proposed hyperspectral RF process  
 154 follows the general approach in [7, 2, 19] and it is depicted in Fig.1. First, the  
 155 user defines a *zero-query* by feeding the system with some positive sample.  
 156 Next, an initial ranking is obtained comparing the database images to the  
 157 query sample by some hyperspectral dissimilarity function and some images  
 158 are retrieved for user's evaluation. Then, the user labels the images retrieved  
 159 by the system, a set of prototype images is selected and the RF process starts.

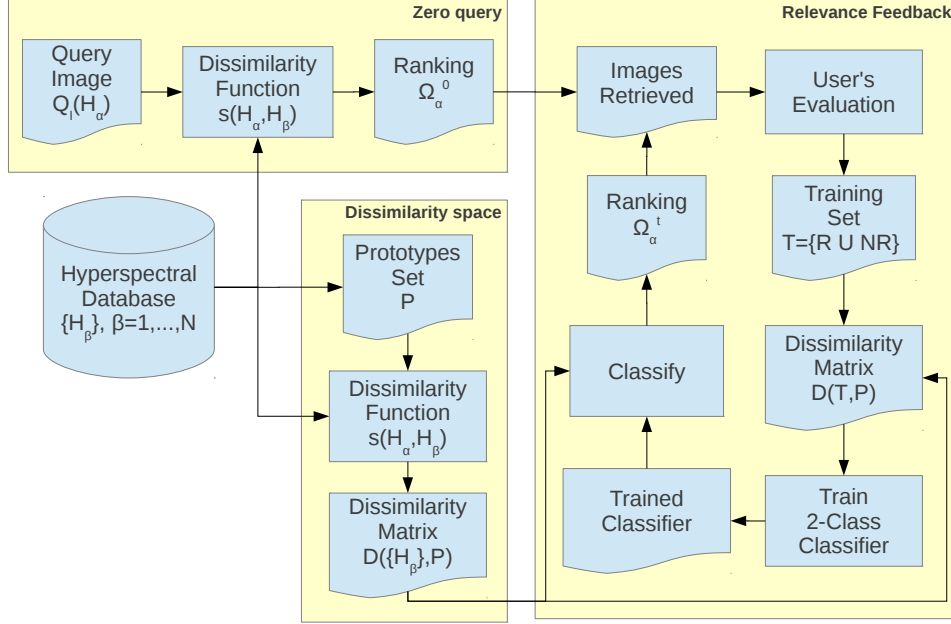


Figure 1: CBIR system diagram with the proposed relevance feedback by dissimilarity spaces approach.

160 We follow by describing the zero-query and the relevance feedback processes  
 161 in detail, and then we discuss on the prototypes selection and the selection  
 162 of the images retrieved by the system for evaluation.

#### 163 4.1. Zero query

164 First, a query  $Q_l(H_\alpha)$  is defined following the query-by-image approach.  
 165  $H_\alpha$  denotes the hyperspectral image selected as the query and  $l \in \mathbb{Z}^+$ , named  
 166 the scope of the query, denotes the number of images that should be retrieved  
 167 by the system. Every image  $H_\beta$  in the dataset is compared to the query image  
 168 by some hyperspectral dissimilarity function,  $s(H_\alpha, H_\beta)$ . The dissimilarities

169 to the query image are represented as a vector  $\mathbf{s}_\alpha = [s_{\alpha,1}, \dots, s_{\alpha,N}]$ , where  $N$   
 170 is the number of images in the dataset and  $s_{\alpha,\beta}$  is the dissimilarity between  
 171 the query image  $H_\alpha$  and the dataset image  $H_\beta$ , with  $\beta = 1, \dots, N$ . Then, we  
 172 sort the components of  $\mathbf{s}_\alpha$  in increasing order, and the resulting shuffled image  
 173 indexes constitute the zero ranking  $\Omega_\alpha^0 = [\omega_q \in \{1, \dots, N\}]$ ,  $q = 1, \dots, N$ , so  
 174 that  $s_{\alpha,\omega_q} \leq s_{\alpha,\omega_{q+1}}$ . Then, some selection criterion is followed to select  $l$   
 175 images from the zero ranking and retrieve them for user’s evaluation. The  
 176 user labels these images as relevant or non-relevant for the query. The set of  
 177 relevant images, denoted as  $R$ , and the set of non-relevant images, denoted  
 178 as  $NR$ , form the training set,  $T = \{R \cup NR\}$ , with which the relevance  
 179 feedback process starts.

#### 180 4.2. Relevance feedback

181 We propose a RF process defined as a two-class problem where the classes  
 182 are the set of relevant (positive class) and the set of irrelevant (negative  
 183 class) images respect to the query. The input to the two-class classifier  
 184 is a feature vector composed of the dissimilarity values computed from a  
 185 given image respect to each of the images of the prototypes set. The output  
 186 of the classifier should be an scalar representing any measure of an image  
 187 identification with the positive class respect to the negative class, for instance  
 188 a class probability. The classifier outputs are ordered to define a ranking of  
 189 the database images respect to the user’s query. Finally, the ranking is used  
 190 to select some database images that will be retrieved for the user’s evaluation  
 191 and so, proceed with a new RF iteration. Thus, the RF process is divided in  
 192 two steps, a training phase and a testing phase.

193 *4.2.1. Training phase*

194 Let  $\mathbf{P} = \{H_{p_i}\}_{i=1}^r$  be the set of prototypes where  $p_i$  is an index pointing  
 195 ing to a database image and  $r$  is the number of prototype instances. Let  
 196  $\mathbf{T} = \{H_{q_j}\}_{j=1}^t$  be the set of training samples where  $q_j$  is an index pointing  
 197 to a database image,  $t$  denotes the number of training samples and each im-  
 198 age  $H_{q_j}$  has been labelled as belonging to the positive class,  $\mathcal{C}^+$ , or to the  
 199 negative class,  $\mathcal{C}^-$ . Then, the system calculates the  $t \times r$  dissimilarity ma-  
 200 trix  $D(\mathbf{T}, \mathbf{P}) = [s(H_{q_j}, H_{p_i})]$ ,  $j = 1, \dots, t$ ,  $i = 1, \dots, r$ ; using some given  
 201 hyperspectral dissimilarity function  $s(\cdot, \cdot)$ . The rows of  $D(\mathbf{T}, \mathbf{P})$  are the geo-  
 202 metrical coordinates of the training samples in the dissimilarity space defined  
 203 by the set of prototypes, and would be used as feature vectors to train the  
 204 two-class classifier.

205 *4.2.2. Testing phase*

206 For each image  $H_\beta$  in the dataset we calculate the dissimilarity vector  $\mathbf{s}_\beta =$   
 207  $D(H_\beta, \mathbf{P}) = [s(H_\beta, H_{p_i})]_{i=1}^r$ , given the hyperspectral dissimilarity function  
 208  $s(\cdot, \cdot)$ . The dissimilarity vector,  $\mathbf{s}_\beta$ , represents a point in the dissimilarity  
 209 space and is used as the input to the trained classifier. The classifier will  
 210 return an scalar,  $c_\beta$ , measuring the probability or the degree of inclusion  
 211 of the image  $H_\beta$  respect to the query class  $\mathcal{C}^+$ . An image  $H_k$  having a  
 212 classification value higher than an image  $H_l$ , that is  $c_k \geq c_l$ , should be ranked  
 213 in a better position. The values obtained by the classifier for all the images  
 214 in the dataset are then represented as a vector  $\mathbf{c}_\alpha = [c_1, \dots, c_N]$ , where  $N$  is  
 215 the number of images in the dataset. The vector of classification values  $\mathbf{c}_\alpha$  is  
 216 sorted in decreasing order and the resulting shuffled image indexes constitute  
 217 the ranking  $\Omega_\alpha^t = [\omega_q^t \in \{1, \dots, N\}]$ ,  $q = 1, \dots, N$ , so that  $c_{\omega_q^t} \geq c_{\omega_{q+1}^t}$ . The

218 superscript  $t$  in  $\Omega_\alpha^t$  denotes the iteration in turn on the RF process, being  
219  $t$  a positive integer,  $t > 0$ . The ranking serves to select some images that  
220 are retrieved to the user for evaluation, and then included in the training  
221 set. The RF process ends when the user is satisfied, a maximum number of  
222 iterations,  $t_{\max}$ , is achieved, or no new images are being incorporated to the  
223 training set.

#### 224 4.3. Prototypes selection

225 The general RF process depicted in Fig.1 requires of a set of prototypes.  
226 We distinguish between two criteria to build the prototypes set, an offline  
227 selection and an online selection. In the former, the prototypes are *a priori*  
228 representative subset of the images in the database. A common procedure is  
229 to perform a clustering and keep the centres of the clusters as the prototypes.  
230 This criterion could lead to a dramatical reduction in the computational  
231 costs of the CBIR system, but on the other hand it defines a fixed set of  
232 prototypes for all the possible queries, limiting the adaptability of the CBIR  
233 system. The later builds the set of prototypes during the RF process. In  
234 each iteration some images are retrieved to the user for evaluation and then  
235 included on the training set. These same images or a subset of them are also  
236 used as prototypes. This allows to adapt the set of prototypes to the query.  
237 However, it increases the computational burden.

#### 238 4.4. Image retrieval

239 A key aspect of RF-CBIR systems is the criterion to select from a given  
240 ranking those images that will be retrieved to the user for evaluation. Let  $l$   
241 denote the scope of the query, that is, the number of images that should be

242 retrieved to the user. If the criterion is to return the best  $l$  images given by the  
243  $l$  best ranked images on the database, is likely that the training set is biased  
244 towards the positive class. So, a better criterion seems to retrieve the  $l/2$   
245 best images and the  $l/2$  worst images, hereafter denoted as the *Best-Worst*  
246 (BW) criterion. However, the best and worst images are not necessarily the  
247 most informative ones. The active learning paradigm [3] states that the most  
248 ambiguous images, those that are close to the class boundaries, are the most  
249 informative. Thus, the *Active Learning* (AL) criterion will return the  $l/2$   
250 most ambiguous images labelled as belonging to the positive class, and the  
251  $l/2$  most ambiguous images labelled as belonging to the negative class.

## 252 5. Experimental methodology

### 253 5.1. Dataset

254 The hyperspectral HyMAP data was made available from HyVista Corp.  
255 and German Aerospace Center’s (DLR) optical Airborne Remote Sensing  
256 and Calibration Facility service<sup>1</sup>. The scene corresponds to a flight line  
257 over the facilities of the DLR center in Oberpfaffenhofen (Germany) and its  
258 surroundings, mostly fields, forests and small towns. The data cube has 2878  
259 lines, 512 samples and 125 spectral bands. We have removed non-informative  
260 bands due to atmospheric absorption and 113 spectral bands remained.

261 We cut the scene in patches of  $64 \times 64$  pixels size for a total of 360 patches  
262 forming the hyperspectral database used in the experiments. We grouped the  
263 patches by visual inspection in five rough categories. The three main cat-

---

<sup>1</sup><http://www.OpAiRS.aero>

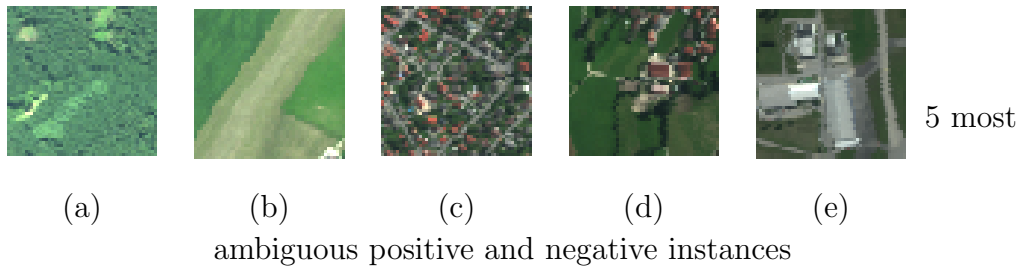


Figure 2: Examples of the five categories patches: (a) Forests, (b) Fields, (c) Urban Areas, (d) Mixed, (e) Others.

264 egories are 'Forests', 'Fields' and 'Urban Areas', representing patches that  
 265 mostly belong to one of this categories. A 'Mixed' category was defined for  
 266 those patches that presented more than one of the three main categories, be-  
 267 ing not any of them dominant. Finally, we defined a fifth category, 'Others',  
 268 for those patches that didn't represent any of the above or that were not  
 269 easily categorized by visual inspection. The number of patches per category  
 270 are: (1) Forests: 39, (2) Fields: 160, (3) Urban Areas: 24, (4) Mixed: 102,  
 271 and (5) Others: 35. Figure 2 shows examples of the five categories patches.

## 272 5.2. Methodology

273 We test the use of the proposed hyperspectral RF-CBIR using the un-  
 274 mixing and dictionary-based hyperspectral dissimilarity functions. For the  
 275 unmixing-based dissimilarities, the spectral (2) and the spectral-spatial (3)  
 276 dissimilarity functions, we conduct for each image in the database an un-  
 277 mixing process in order to obtain the set of induced endmembers and their  
 278 corresponding fractional abundances. In order to do that we use the Vertex  
 279 Component Analysis (VCA) [18] endmember induction algorithm and a par-  
 280 tially constrained least squares unmixing (PCLSU) [12] algorithm. As VCA

281 is an stochastic algorithm we perform 20 independent runs for each image and  
 282 we keep the one with the lowest averaged root squared mean reconstruction  
 283 error:

$$\epsilon(H, \hat{H}) = \frac{1}{M} \sum_{i=1}^M \sqrt{\frac{1}{q} \sum_{j=1}^q (H_i^{(j)} - \hat{H}_i^{(j)})^2} \quad (5)$$

284 where  $H_i^{(j)}$  denotes the  $j$ -th band value of the  $i$ -th pixel in the hyperspectral  
 285 image  $H$  and  $\hat{H} = \Phi \mathbf{E}$  is the hyperspectral image reconstructed by the set  
 286 of induced endmembers  $\mathbf{E}$  and their corresponding fractional abundances  $\Phi$ .  
 287 For the Normalized Dictionary Distance (4), we first convert each hyperspec-  
 288 tral image to a text string in two ways, using the average of the spectral bands  
 289 and band-by-band. For the former, we calculate the mean of each hyperspec-  
 290 tral pixel along the spectral bands. For the later we transform each spectral  
 291 band independently. In both cases we traverse the image in a zig-zag way.  
 292 The averaged band transformation incurs in a big lost of spectral information  
 293 compared to the band by band transformation, but by contrast it yields to  
 294 a more compact dictionary and so, to speed up the NDD computation.

295 Thus, we compare the use of the four hyperspectral dissimilarities, the  
 296 Spectral, the Spectral-Spatial, the Averaged Band NDD and the Band-by-  
 297 Band NDD, in the RF process respect to their use in the zero-query. In  
 298 order to do that, we run independent retrieval experiments over the HyMAP  
 299 dataset. Each of the 360 patches was *a priori* labelled as belonging to one  
 300 of the five categories defined above. The query is a categorical search, where  
 301 the images belonging to the same category than the query image form the  
 302 positive class and the remaining ones form the negative class. We perform  
 303 an independent search for each of the 360 patches. Thus, user’s evaluation

304 was not required and the experiment was fully automatized. The maximum  
 305 number of iterations on the retrieval feedback process was set to  $t_{\max} = 5$ .

306 For the RF process we compare the use of a  $k$ -NN classifier and a two-class  
 307 SVM classifier with a radial basis kernel. The  $k$ -NN classifier does not require  
 308 of a training phase and returns the fraction of the  $k$  most similar images in  
 309 the training set respect to the query image belonging to the positive class,  
 310 that is,  $c = \frac{\sum_{i=1}^k I(H_i, H_\alpha)}{k}$ , where  $I$  denotes an indicator function returning 1 if  
 311 the two images belong to the same class, and 0 otherwise. The SVM classifier  
 312 outputs the probability that the tested image belongs to the positive class.  
 313 The parameters of the SVM classifier were selected using a 5-fold cross  
 314 validation. For the  $k$ -NN the *knnclassify* MATLAB function was used. For  
 315 the SVM, we used the  $C$ -SVM classifier of the LIBSVM [3] library.

316 We also compare the use of online and offline prototypes selection pro-  
 317 cesses. For the offline prototypes selection process we performed a hierarchi-  
 318 cal segmentation using each of the four hyperspectral dissimilarity functions  
 319 and we keep 10 clusters. Then, for each cluster  $\zeta$  we selected the image  $H_\zeta^o$   
 320 minimizing the averaged distance to the rest of images grouped into the same  
 321 cluster:

$$H_\zeta^o = \arg \min_i \frac{1}{|\zeta|} \sum_{H_j \in \zeta} s(H_i, H_j) \quad (6)$$

322 where  $|\zeta|$  denotes the cardinality of the cluster  $\zeta$ .

323 Finally, we compare the results obtained using three different criteria to  
 324 select the images to be retrieved to the user for evaluation: the BW criterion,  
 325 the AL criterion and a combination of both, BW+AL. For the BW criterion  
 326 the system retrieves the 5 best and worst ranked images in the database.  
 327 For the AL criterion the system retrieves the 5 most ambiguous positive and

328 negative instances, that is, the ones closed to the class boundary on each side.  
 329 For both, BW and AL criteria, the scope is then  $l = 10$ . For the BW+AL  
 330 criterion the system returns the 3 best and worst ranked images, and the 3  
 331 most ambiguous positive and negative instances, for a total scope of  $l = 12$ .

### 332 5.3. Performance measures

333 Evaluation metrics from information retrieval field have been adopted  
 334 to evaluate CBIR systems quality. The two most used evaluation measures  
 335 are *precision* and *recall* [25, 4]. Precision,  $p$ , is the fraction of the returned  
 336 images that are relevant to the query. Recall,  $q$ , is the fraction of retrieved  
 337 relevant images respect to the total number of relevant images in the database  
 338 according to *a priori* knowledge. If we denote  $L$  the set of returned images  
 339 and  $R$  the set of all the images relevant to the query, then  $p = \frac{|L \cap R|}{|L|}$  and  
 340  $r = \frac{|L \cap R|}{|R|}$ . Precision and recall follow inverse trends when considered as  
 341 functions of the scope of the query. Precision falls while recall increases as  
 342 the scope increases. Thus, precision and recall measures are usually given as  
 343 precision-recall curves for a fixed scope. To evaluate the overall performance  
 344 of a CBIR system, the Average Precision and Average Recall are calculated  
 345 over all the query images in the database. For a query of scope  $l$ , these are  
 346 defined as:

$$\bar{p}_l = \frac{1}{N} \sum_{\alpha=1}^N p_l(H_\alpha) \quad (7)$$

347 and

$$\bar{r}_l = \frac{1}{N} \sum_{\alpha=1}^N r_l(H_\alpha). \quad (8)$$

348 The Normalized Rank [17] was used to summarize the system performance  
 349 into an scalar value. The normalized rank for a given image query, denoted

350 as Rank ( $H_\alpha$ ), is defined as:

$$\text{Rank}(H_\alpha) = \frac{1}{NN_\alpha} \left( \sum_{i=1}^{N_\alpha} \Omega_\alpha^i - \frac{N_\alpha(N_\alpha - 1)}{2} \right), \quad (9)$$

351 where  $N$  is the number of images in the dataset,  $N_\alpha$  is the number of rele-  
352 vant images for the query  $H_\alpha$ , and  $\Omega_\alpha^i$  is the rank at which the  $i$ -th image  
353 is retrieved. This measure is 0 for perfect performance, and approaches 1  
354 as performance worsens, being 0.5 equivalent to a random retrieval. We cal-  
355 culated the Rank ( $H_\alpha$ ) for each of the images in the dataset and then we  
356 calculated the average normalized rank (ANR):

$$ANR = \frac{1}{N} \sum_{\alpha=1}^N \text{Rank}(H_\alpha). \quad (10)$$

## 357 6. Results

358 Tables 2-3 show the ANR (10) values of the comparing hyperspectral dis-  
359 similarities, using the proposed RF-CBIR respect to the zero-query, for the  
360 Forest, Fields and Urban areas categorical queries respectively. We run the  
361 experiments using different values of  $k$  for the  $k$ -NN classifier, but we only  
362 show the results using  $k = 7$  as in general it outperforms the other  $k$  values.  
363 The ANR results correspond to the ranking obtained in the fifth RF itera-  
364 tion. In general, the hyperspectral RF process yields to better ANR results  
365 than the zero query for the four compared hyperspectral dissimilarity func-  
366 tions. The online prototype selection leads to better results than the offline  
367 selection, and so it does the 7-NN classifier compared to the SVM classifier.  
368 The use of AL for the image retrieval selection outperforms the BW criterion,  
369 and often the combination of both, BW+AL. As it was expected, the results

Table 1: ANR values of the hyperspectral RF-CBIR for the Forests categorical search.

			Avg.Band NDD	By-Band NDD	Spectral	Spectral-Spatial
Zero Query			0.0809	0.0613	0.1360	0.0552
Online Prot.	7NN	BW	0.0343	0.0426	0.1394	0.0630
		AL	<b>0.0280</b>	<b>0.0258</b>	0.0869	0.0337
		BW+AL	0.0287	0.0281	<b>0.0770</b>	<b>0.0330</b>
	SVM	BW	0.0383	0.1392	0.2600	0.0852
		AL	0.0596	0.1155	0.3947	0.2371
		BW+AL	0.0462	0.0358	0.2143	0.2430
Offline Prot.	7NN	BW	0.0662	0.0723	0.1922	0.0543
		AL	0.0329	0.0631	0.1735	0.0494
		BW+AL	0.0448	0.0633	0.1848	0.0473
	SVM	BW	0.0758	0.0478	0.2502	0.1063
		AL	0.0542	0.0409	0.3116	0.1678
		BW+AL	0.0642	0.0538	0.3180	0.1055

370 using the Band-by-Band NDD and the Spectral-Spatial dissimilarity func-  
 371 tions outperform the Averaged Bands NDD and the Spectral dissimilarity  
 372 functions.

373 There are however some discrepancies depending on the categorical query.  
 374 This effect is specially relevant for the Urban areas category and it is related  
 375 to the asymmetry in the number of images present in the database for each  
 376 class. The low number of images belonging to the Urban areas category  
 377 makes the training set very unbalanced yielding to poor classification re-  
 378 sults, and so, to a low performance in the CBIR ranking. Figures 4-5 show

Table 2: ANR values of the hyperspectral RF-CBIR for the Fields categorical search.

			Avg.Band NDD	By-Band NDD	Spectral	Spectral-Spatial
Zero Query			0.2171	0.1641	0.1594	0.1599
Online Prot.	7NN	BW	0.1552	0.0634	0.1776	0.1494
		AL	<b>0.1388</b>	<b>0.0495</b>	0.1573	0.1514
		BW+AL	0.1433	0.0587	0.1862	0.1883
	SVM	BW	0.1898	0.2462	0.1511	0.1983
		AL	0.1808	0.0914	0.1526	<b>0.0924</b>
		BW+AL	0.1567	0.0812	<b>0.1477</b>	0.1184
Offline Prot.	7NN	BW	0.1847	0.0756	0.2607	0.1779
		AL	0.1802	0.0533	0.2660	0.2158
		BW+AL	0.1694	0.0569	0.2957	0.1994
	SVM	BW	0.2033	0.0724	0.2136	0.1936
		AL	0.1831	0.0660	0.2112	0.1700
		BW+AL	0.2008	0.0497	0.2171	0.1442

Table 3: ANR values of the hyperspectral RF-CBIR for the Urban areas categorical search.

			Avg.Band NDD	By-Band NDD	Spectral	Spectral-Spatial
Zero Query			<b>0.1217</b>	<b>0.0080</b>	0.2068	0.0732
Online Prot.	7NN	BW	0.1920	<b>0.0082</b>	<b>0.0509</b>	0.0416
		AL	0.1900	0.0096	0.0626	<b>0.0392</b>
		BW+AL	0.2702	0.0282	0.1230	0.0654
	SVM	BW	0.2675	0.0437	0.1120	0.2126
		AL	0.5870	0.0416	0.2501	0.1603
		BW+AL	0.3825	0.0415	0.1459	0.1712
Offline Prot.	7NN	BW	0.2578	0.0545	0.0799	0.0762
		AL	0.2713	0.0276	0.0698	0.0570
		BW+AL	0.3425	0.1061	0.1509	0.1224
	SVM	BW	<b>0.1562</b>	0.0103	0.0833	0.1240
		AL	0.2276	0.0273	0.2164	0.2651
		BW+AL	0.1763	0.0246	0.0561	0.2032

379 the average number of relevant (R) and non-relevant (NR) images in the  
380 training set for each RF iteration using the BW and the AL image retrieval  
381 selection criteria for the Forests, Fields and Urban areas categorical queries  
382 respectively. It is clear that the Urban areas category presents the most  
383 asymmetrical distribution of the training set into relevant and non-relevant  
384 images, what it can explain the poor results on the RF process for this cat-  
385 egory. In general, the asymmetry in the R/NR ratio is not so important as  
386 soon as there are some critical number of each on the training set. It is also  
387 possible to observe that the AL selection criterion yields to better training  
388 sets compared to the BW selection criterion, expressed as bigger and more  
389 equally distributed training sets. This issue seems to be a major drawback  
390 for the SVM classifier while the impact on the 7-NN classifier is less severe as  
391 soon as there are enough positive samples present on the training set. This  
392 issue should be further addressed in future research in order to develop an  
393 operative hyperspectral RF-CBIR system.

394 Finally, Figures 6 and 7 show the P-R curves (7) (8) for the zero-query  
395 and the best RF results respectively, using the four comparing dissimilarity  
396 functions. The improve on the P-R curves by the RF process is clear except  
397 for the Urban areas categorical search, due to the pernicious effect of the lack  
398 of positive samples and the consequent asymmetrical distribution of R/NR  
399 samples on the training sets.

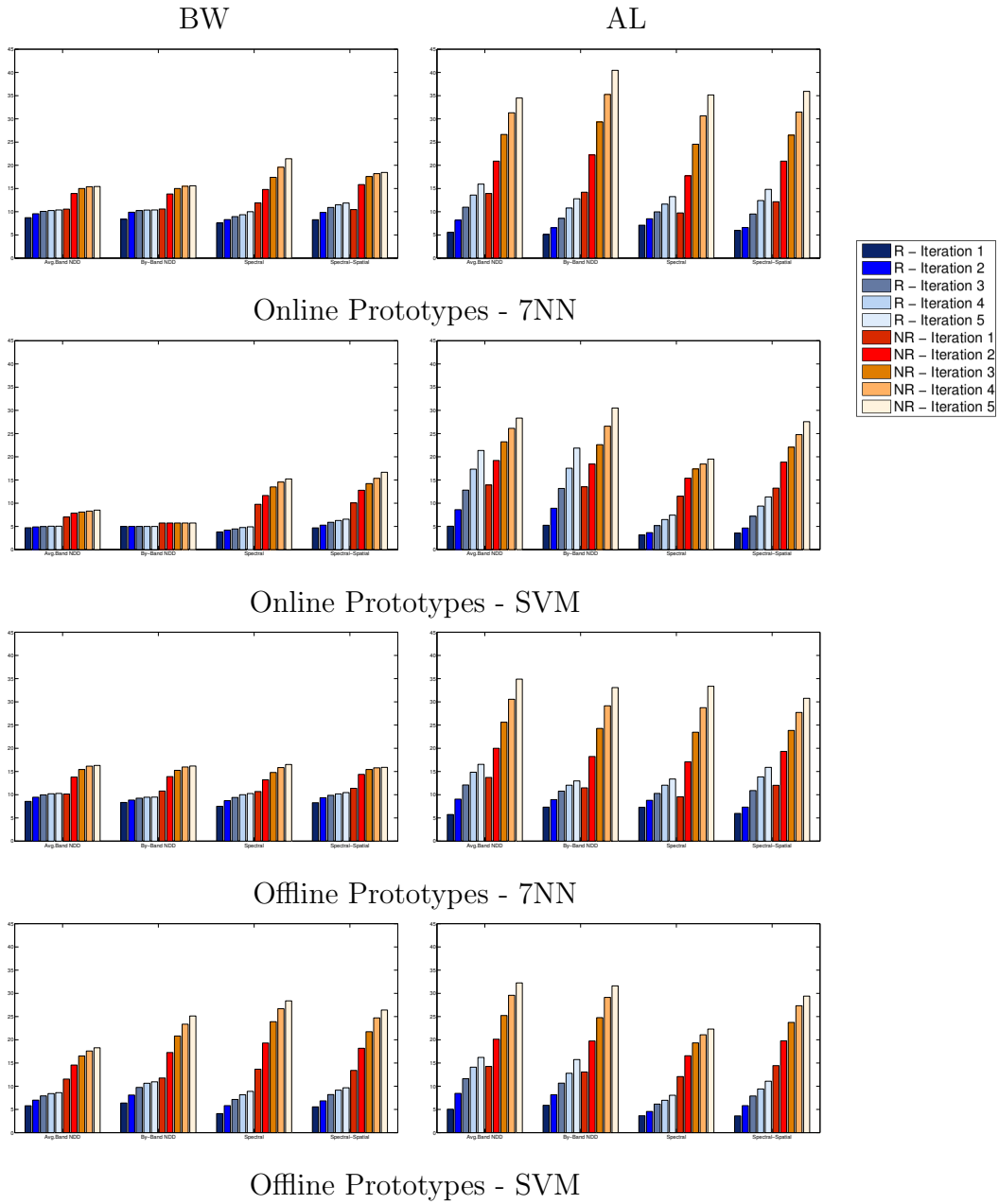


Figure 3: Average number of relevant (R) and non-relevant (NR) images in the training set for each RF iteration and comparing hyperspectral dissimilarity functions, using the BW and the AL image retrieval selection criteria for the Forests categorical search.

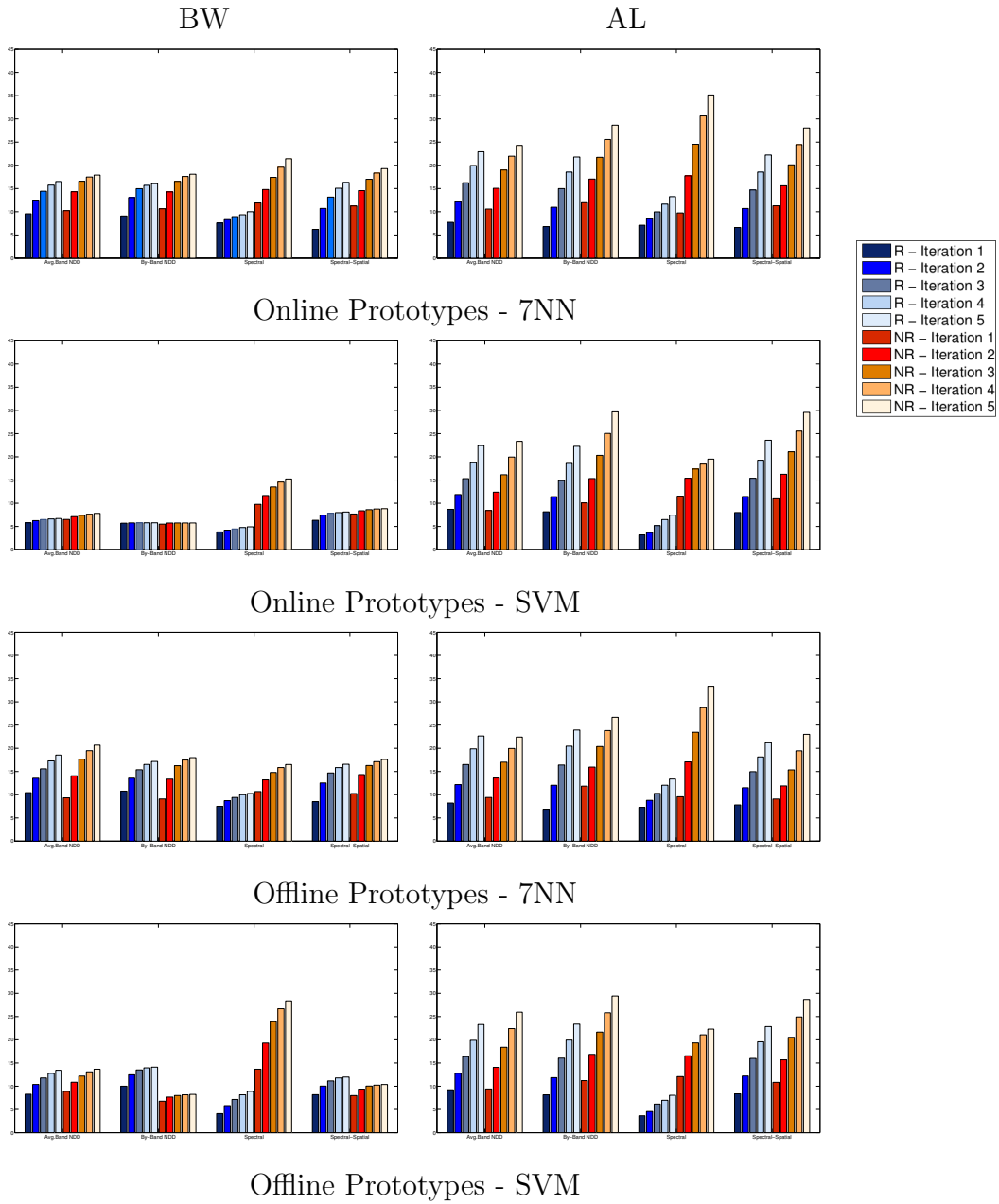


Figure 4: Average number of relevant (R) and non-relevant (NR) images in the training set for each RF iteration and comparing hyperspectral dissimilarity functions, using the BW and the AL image retrieval selection criteria for the Fields categorical search.

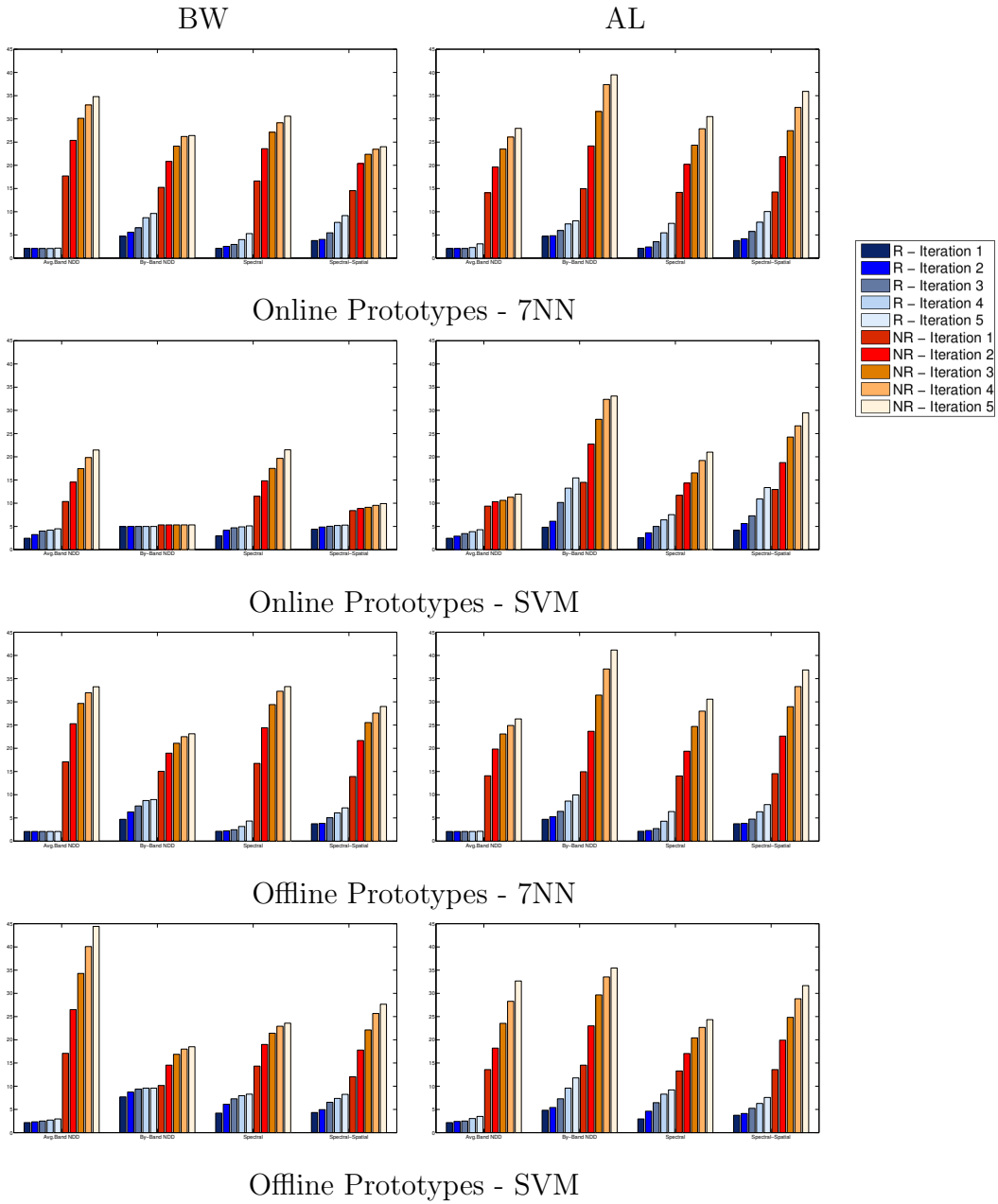


Figure 5: Average number of relevant (R) and non-relevant (NR) images in the training set for each RF iteration and comparing hyperspectral dissimilarity functions, using the BW and the AL image retrieval selection criteria for the Urban areas categorical search.

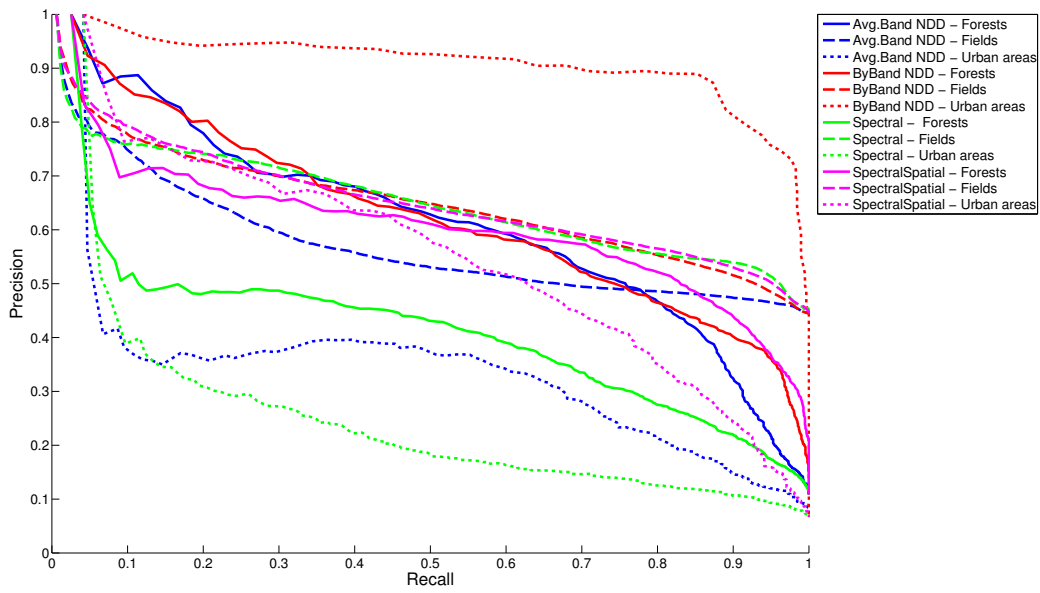


Figure 6: Precision-Recall curves for the zero query.

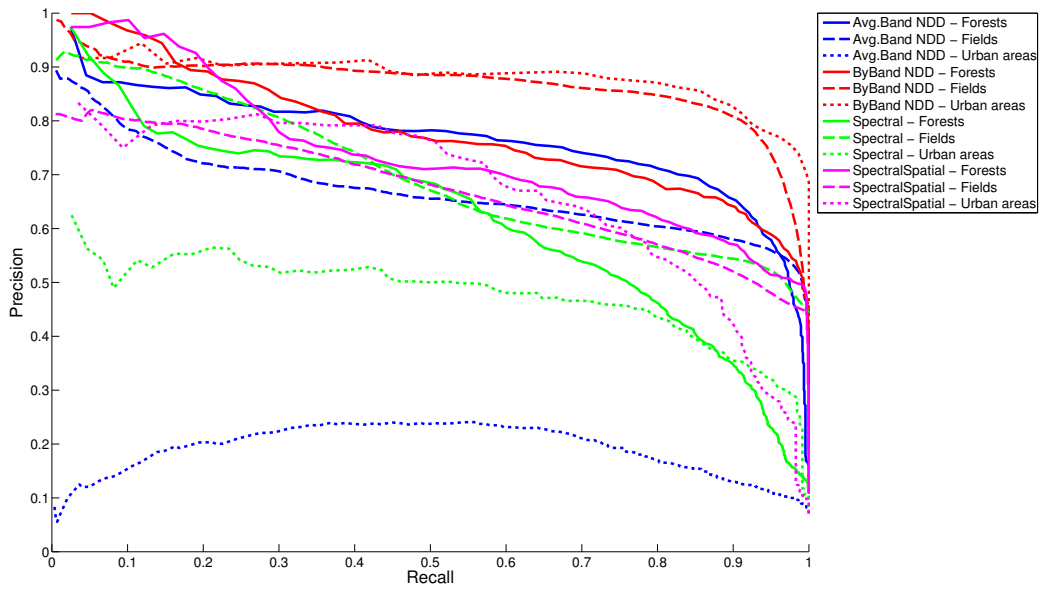


Figure 7: Precision-Recall curves for the best RF results.

## 400 **7. Conclusions**

401 We have extended the hyperspectral CBIR systems present on the liter-  
402 ature by a RF process based on dissimilarity spaces. To define a relevance  
403 feedback process for hyperspectral CBIR systems is not easy as most of the  
404 available hyperspectral CBIR systems rely on feature representations and  
405 dissimilarity functions that do not fulfil the conditions to be used in com-  
406 mon machine learning RF processes. The proposed approach expands the  
407 available dissimilarity-based hyperspectral CBIR systems on the literature  
408 in a simple way by using dissimilarity space instead of the usual feature  
409 space. The proposed approach proved to improve the performance of the hy-  
410 perspectral CBIR systems in the preliminary experiments presented on this  
411 paper. Also, the selection of a proper training set for the RF process was  
412 pointed as a major issue affecting the performance of the proposed hyper-  
413 spectral RF-CBIR system. Further research will focus on this aspect and on  
414 the validation of the proposed system in a real scenario with a big database  
415 of hyperspectral images and real users.

## 416 **Acknowledgements**

417 The authors very much acknowledge the support of Dr. Martin Bachmann  
418 from DLR.

## 419 **References**

- 420 [1] J.M. Bioucas-Dias, A. Plaza, N. Dobigeon, M. Parente, Qian Du,  
421 P. Gader, and J. Chanussot. Hyperspectral unmixing overview: Ge-  
422 ometrical, statistical, and sparse regression-based approaches. *IEEE*

- 423 *Journal of Selected Topics in Applied Earth Observations and Remote*  
424 *Sensing*, 5(2):354–379, 2012.
- 425 [2] E. Bruno, N. Moenne-Loccoz, and S. Marchand-Maillet. Learning user  
426 queries in multimodal dissimilarity spaces. In M. Detyniecki, J.M. Jose,  
427 A. Nurnberger, and C.J. Rijsbergen, editors, *Adaptive Multimedia Re-*  
428 *trieval: User, Context, and Feedback*, volume 3877 of *Lecture Notes in*  
429 *Computer Science*, pages 168–179. Springer Berlin Heidelberg, 2006.
- 430 [3] C.-C. Chang and C.-J. Lin. LIBSVM: A library for support vector  
431 machines. *ACM Transactions on Intelligent Systems and Technology*,  
432 2:27:1–27:27, 2011.
- 433 [4] H. Daschiel and M. Datcu. Information mining in remote sensing image  
434 archives: system evaluation. *Geoscience and Remote Sensing, IEEE*  
435 *Transactions on*, 43(1):188–199, 2005.
- 436 [5] R.P.W. Duin and E. Pekalska. The dissimilarity space: Bridging struc-  
437 tural and statistical pattern recognition. *Pattern Recognition Letters*,  
438 33(7):826 – 832, 2012.
- 439 [6] German Spatial Agency (DLR). Environmental mapping and analysis  
440 program (enmap), 2011.
- 441 [7] G. Giacinto and F. Roli. Dissimilarity representation of images for rel-  
442 evance feedback in content-based image retrieval. In P. Perner and  
443 A. Rosenfeld, editors, *Machine Learning and Data Mining in Pattern*  
444 *Recognition*, volume 2734 of *Lecture Notes in Computer Science*, pages  
445 202–214. 2003.

- 446 [8] Manuel Graña and Miguel A. Veganzones. An endmember-based dis-  
447 tance for content based hyperspectral image retrieval. *Pattern Recogni-*  
448 *tion*, 45(9):3472 – 3489, 2012.
- 449 [9] Italian Spatial Agency (ASI). Precursore iperspettrale of the application  
450 mission (prisma), 2011.
- 451 [10] N. Keshava and J. F Mustard. Spectral unmixing. *IEEE Signal Pro-*  
452 *cessing Magazine*, 19(1):44–57, January 2002.
- 453 [11] N. Keshava and J.F. Mustard. Spectral unmixing. *Signal Processing*  
454 *Magazine, IEEE*, 19(1):44–57, 2002.
- 455 [12] Charles L. Lawson. *Solving Least Squares Problems*. Prentice Hall, 1974.
- 456 [13] J. Li, J.Z. Wang, and G. Wiederhold. IRM: integrated region matching  
457 for image retrieval. In *Proceedings of the eighth ACM international*  
458 *conference on Multimedia*, MULTIMEDIA '00, pages 147–156, Marina  
459 del Rey, California, United States, 2000. ACM.
- 460 [14] Ming Li, Xin Chen, Xin Li, Bin Ma, and P.M.B. Vitanyi. The similarity  
461 metric. *IEEE Transactions on Information Theory*, 50(12):3250–3264,  
462 2004.
- 463 [15] Ming Li and Paul Vitanyi. *An Introduction to Kolmogorov Complexity*  
464 *and Its Applications*. Springer, 2nd edition, February 1997.
- 465 [16] A. Macedonas, D. Besiris, G. Economou, and S. Fotopoulos. Dictio-  
466 nary based color image retrieval. *Journal of Visual Communication and*  
467 *Image Representation*, 19(7):464–470, 2008.

- 468 [17] H. Muller, W. Muller, D.McG. Squire, S. Marchand-Maillet, and T. Pun.  
469 Performance evaluation in content-based image retrieval: overview and  
470 proposals. *Pattern Recognition Letters*, 22(5):593–601, 2001.
- 471 [18] J.M.P. Nascimento and J.M. Bioucas Dias. Vertex component analysis:  
472 a fast algorithm to unmix hyperspectral data. *IEEE Transactions on*  
473 *Geoscience and Remote Sensing*, 43(4):898–910, 2005.
- 474 [19] G.P. Nguyen, M. Worring, and A.W.M. Smeulders. Similarity learn-  
475 ing via dissimilarity space in cbir. In *ACM International Multimedia*  
476 *Conference and Exhibition*, pages 107–116, 2006.
- 477 [20] E. Pekalska and Robert P.W. Duin. *The Dissimilarity Representation*  
478 *for Pattern Recognition: Foundations And Applications*. World Scientific  
479 Pub Co Inc, 2005.
- 480 [21] E. Pekalska and B. Haasdonk. Kernel discriminant analysis for positive  
481 definite and indefinite kernels. *IEEE Transactions on Pattern Analysis*  
482 *and Machine Intelligence*, 31(6):1017–1032, 2009.
- 483 [22] A. Plaza, P. Martinez, R. Perez, and J. Plaza. A quantitative and  
484 comparative analysis of endmember extraction algorithms from hyper-  
485 spectral data. *IEEE Transactions on Geoscience and Remote Sensing*,  
486 42(3):650–663, 2004.
- 487 [23] Antonio Plaza, Jon Atli Benediktsson, Joseph W. Boardman, Jason  
488 Brazile, Lorenzo Bruzzone, Gustavo Camps-Valls, Jocelyn Chanussot,  
489 Mathieu Fauvel, Paolo Gamba, Anthony Gualtieri, Mattia Marconcini,  
490 James C. Tilton, and Giovanna Trianni. Recent advances in techniques

- 491 for hyperspectral image processing. *Remote Sensing of Environment*,  
492 113, Supplement 1(0):S110–S122, September 2009.
- 493 [24] J. Shawe-Taylor and N. Cristianini. *Kernel methods for pattern analysis*.  
494 Cambridge University Press, 2004.
- 495 [25] A.W.M. Smeulders, M. Worring, S. Santini, A. Gupta, and R. Jain.  
496 Content-based image retrieval at the end of the early years. *IEEE Trans-*  
497 *actions on Pattern Analysis and Machine Intelligence*, 22(12):1349–  
498 1380, 2000.
- 499 [26] M. A. Veganzones and M. Graña. Endmember extraction methods: A  
500 short review. In *Knowledge-Based Intelligent Information and Engineer-*  
501 *ing Systems, 12th International Conference, KES 2008, Zagreb, Croa-*  
502 *tia, September 3-5, 2008, Proceedings, Part III*, volume 5179 of *Lecture*  
503 *Notes in Computer Science*, pages 400–407. Springer, 2008.
- 504 [27] M.A. Veganzones, M. Datcu, and M. Graña. Dictionary based hyper-  
505 spectral image retrieval. In *Proceedings of the 1st International Confer-*  
506 *ence on Pattern Recognition Applications and Methods*, pages 426–432.  
507 SciTePress, 2012.
- 508 [28] M.A. Veganzones and M. Graña. A spectral/spatial cbir system for  
509 hyperspectral images. *IEEE Journal of Selected Topics in Applied Earth*  
510 *Observations and Remote Sensing*, 5(2):488–500, april 2012.
- 511 [29] T. Watanabe, K. Sugawara, and H. Sugihara. A new pattern represen-  
512 tation scheme using data compression. *IEEE Transactions on Pattern*  
513 *Analysis and Machine Intelligence*, 24(5):579–590, 2002.

- 514 [30] T.A. Welch. A technique for high-performance data compression. *Com-*  
515 *puter*, 17(6):8–19, 1984.
- 516 [31] Xiang Sean Zhou and Thomas S. Huang. Relevance feedback in image  
517 retrieval: A comprehensive review. *Multimedia Systems*, 8(6):536–544,  
518 2003.